Noise effect on the interpolation equation for near infrared thermography

Thierry Sentenac, Rémi Gilblas

Noise effect on the interpolation equation for near infrared thermography

Thierry Sentenac[1,2] **and Rémi Gilblas**[1]

[1] Université de Toulouse; INSA, UPS, Mines Albi, ISAE, ICA (Institut Clément Ader); Campus Jarlard, F-81013 Albi cedex 09, France
[2] CNRS; LAAS; 7 avenue du Colonel Roche, F-31077 Toulouse, France

E-mail: sentenac@mines-albi.fr

Abstract
This paper investigates the performance of interpolation equations for a near infrared thermal imager operating over wavelengths from 0.9 µm to 1.7 µm with various filter bandwidths and a broad temperature range from 300 °C to 1000 °C. The equations are based on a general formulation of the effective wavelength as a function of the temperature. The quality of the interpolation is assessed in relation to the order of the effective wavelength. However, the noise induced by the imperfections of the thermal imager significantly disturbs the signal, and this phenomenon is enhanced as the bandwidth of the filter increases (i.e. for low-temperature applications). The main purpose of this paper is to establish the right choice of the filter bandwidth and the expression and order of the interpolation equation in relation to the noise level on the thermal imager and the desired accuracy. This paper first outlines the background on interpolation equations and then tests them on synthetic data from signals delivered first by an ideal thermal imager (i.e. free from noise) and then from noisy signals. This simulation study provides a framework for users to select an interpolation equation with an adequate order for near infrared thermal imagers. The performances of the selected interpolation equations are finally demonstrated on real images performed by a near infrared thermal imager.

1. Introduction

An accurate on-line temperature measurement is the key parameter for the optimization and quality assurance of many industrial processes. Non-contact infrared systems, such as pyrometers and thermal imagers, are suitable in many industrial applications or research projects. For temperatures ranging from 300 °C to 1000 °C, near infrared thermal imagers, operating at short wavelengths (from 0.9 µm to 1.7 µm), provide high performances in terms of temperature sensitivity, and also have the advantage of being less sensitive to emissivity. Furthermore, they deliver images with a high spatial resolution which is suitable for studies on materials with non-uniform surfaces. These thermal imagers are then widely used for thermal imaging applications [1], for radiance temperature measurements [2], for multi-spectral measurements [3, 4] and for true temperature field measurements [5].

For these applications, it is essential that a radiometric calibration of the thermal imager is carried out with low temperature error [6]. The signal of the thermal imager is the integral of its spectral responsivity multiplied by the spectral radiance of the black body. An ideal radiometric calibration requires the measurement of the spectral responsivity of the thermal imager and the integration of Planck's law over its spectral bandwidth. Unfortunately, the spectral responsivity provided by the manufacturer is often given as a relative value.

When the spectral responsivity of the thermal imager is unknown, an algebraic interpolation equation approximates the relationship between the output signal of the thermal imager and the temperature of the black body. The calibration parameters of the interpolation equation are estimated by a common multi-point calibration method based on least-squares fitting of the measured output signals versus the different temperatures of the black body. Then, the difference between the estimated temperature obtained by inverting the interpolation equation and the true black-body temperature is known as the interpolation error. It should ideally be smaller than about $1/3$ to $1/5$ of the quadrature sum of all the other uncertainty components of the radiometric calibration.

Hence, it should ideally be comparable to the accuracy of the black-body temperature (around 0.1 °C). Therefore, the interpolation equation should not introduce additional errors and the interpolation error should not impact the total uncertainty. In this secondary radiometric calibration approach to thermal imagers, performed with a multi-point method using interpolation equations, choosing a proper interpolation equation is a fundamental step to minimize the interpolation error.

The easiest interpolation equation is the monochromatic approximation of the product of black-body radiance in Planck or Wien formulation by the thermal imager responsivity around a mean operating wavelength. The suitability of this equation depends on the temperature range, the spectral bandwidth of the thermal imager and the required accuracy of the application. As shown in [7], the monochromatic approximation introduces large interpolation errors in the near infrared spectral band, which is not acceptable for many applications. This error can be reduced by adding correction factors used with a reference wavelength [8] and at high temperatures (above 1500 °C) [9]. However, the estimated temperature calculated from this interpolation equation cannot be derived analytically. In contrast, the Sakuma–Hattori [10] interpolation equation, based on a temperature-dependent effective wavelength, which is a polynomial function at first order of the temperature, is analytically invertible. However, this equation is fitted using non-linear least-squares techniques. An interpolation equation with a general formulation of the inverse effective wavelength as a polynomial function at various orders of the inverse temperature, suggested in [11], can easily be fitted using linear least-squares techniques when this interpolation equation is expressed with the Wien approximation. Moreover, a physical interpretation of the calibration parameters is provided.

This paper addresses the issue of the choice of an interpolation equation with this final formulation of a temperature-dependent effective wavelength for a near infrared thermal imager equipped for various filters representing different applications of near infrared thermography and operating over a broad temperature range (300 °C–1000 °C). With respect to [12], the paper assesses the interpolation errors for an ideal thermal imager (i.e. free from noise) to study the error due to the different orders of the effective wavelength and the influence of the filter characteristics. In addition, the interpolation error is investigated from the interpolation equation fitting to noisy data. The interpolation error is then the addition of an error due to the interpolation equation (evaluated from noiseless data) and an error due to the noise in the thermal imager signal. The main objective of this paper is to evaluate the performance of the interpolation error in relation to the level of noise.

This paper is organized as follows: in section 2 the main interpolation equations required for the study are recalled. In section 3, interpolation errors are calculated for simulated data from an ideal near infrared thermal imager equipped with Gaussian filters. The interpolation errors are also given in relation to the noise of the thermal imager signal. Finally, section 4 is devoted to the assessment of the performances of interpolation equations with real data from a near infrared thermal imager with a different bandwidth filter.

2. Background to interpolation equations

This section recalls the fundamental radiometric equation which links the black-body temperature to the thermal imager's signal through the integration of Planck's law and the spectral responsivity of the thermal imager. When this spectral responsivity is unknown, interpolation equations provide a useful alternative by approximating the integral using an analytic function with fitting parameters. This section discusses various definitions of interpolation equations.

2.1. Fundamental radiometric equation

Let us consider a thermal imager, in a dark room, viewing a black-body source at temperature T, with an atmosphere of unitary transmission and without any other heat sources. Then, the output signal I_D, provided by the thermal imager with a linear response, is the integral of the spectral responsivity ($W(\lambda)$) multiplied by the spectral radiance of the black body (defined on a finite bandwidth $\Delta\lambda$):

$$I_D = k \int_{\Delta\lambda} L_0(\lambda, T)\, W(\lambda)\, d\lambda, \tag{1}$$

where k is a constant dependent on geometrical, optical, electrical and digital properties of the thermal imager which is expressed in DL m^2 sr W^{-1} (DL: digital level). This constant can be computed up to a scale factor and for this study it will be set at one. The integration bandwidth $\Delta\lambda$ depends on the thermal imager. The relative spectral responsivity $W(\lambda)$ includes the detector sensitivity and the transmittances of the filter and lens. The spectral radiance of the black body, L_0, is given by Planck's law at wavelength λ and temperature T.

According to equation (1), an ideal radiometric calibration requires the measurement of the spectral responsivity W of the thermal imager and the integration of Planck's law over this spectral responsivity [13]. However, its measurement remains difficult to obtain.

2.2. Principle of the interpolation equation

As a first approach the interpolation equation can be expressed as a monochromatic approximation, based on the mean operating wavelength of the thermal imager (which is the mean wavelength value of the product of filter transmittance and imager responsivity), λ_0, as follows:

$$k \int_{\Delta\lambda} L_0(\lambda, T)\, W(\lambda)\, d\lambda \approx \hat{I}_D = k\Delta\lambda\, L_0(\lambda_0, T)\, W(\lambda_0). \tag{2}$$

The next step can be the choice between Planck's form and Wien's approximation for the expression of the black-body spectral radiance $L_0(\lambda_0, T)$. Wien's approximation is accurate to within 1% if the condition $\lambda T < 3000\,\mu m\,K$ is observed. This choice depends on the temperature range and the spectral band of the thermal imager. For the temperature range 300 °C–1000 °C, considered in our application, the wavelength should be shorter than 2.4 µm. Wien's approximation is then available for our wavelengths (0.9 µm to 1.7 µm) and the simplest

interpolation equation can be expressed as follows:

$$\hat{I}_{\mathrm{D}} = A\ \exp\left(\frac{-C_2}{\lambda_0\, T}\right), \tag{3}$$

where A is a fitting parameter related to the spectral responsivity given by

$$A = k\, C_1 \int_{\Delta\lambda} W(\lambda)\lambda^{-5}\,\mathrm{d}\lambda \approx k\,\Delta\lambda\, C_1\, \lambda_0^{-5}\, W(\lambda_0), \tag{4}$$

C_1 and C_2 are the first and the second radiation constants ($C_1 = 1.191\,042 \times 10^8\,\mathrm{W\,\mu m^4\,m^{-2}}$ and $C_2 = 14\,388\,\mathrm{K\,\mu m}$). Parameter A is assumed to be a property of the thermal imager that depends only on its spectral characteristics and responsivity.

The third step is the calculation of the interpolation error, which is the difference between the estimated temperature provided by the interpolation equation and the black-body temperature. This error is compared with the required accuracy of the application. For example, in the near infrared spectral band, with Wien's formulation, this monochromatic interpolation equation provides an interpolation error greater than 1 °C [14] in the temperature range 300 °C–1000 °C. A correction factor is then usually applied to decrease the interpolation error. A first method is the reference wavelength method [15, 9] which uses a temperature-dependent factor $A(T)$ and a fixed reference wavelength, λ_{r}, in the exponential term (λ_{r} can exhibit a value close to λ_0). However, the estimated temperature calculated from this interpolation equation cannot be derived analytically but only by iteration. In contrast, the effective wavelength method [10] is based on a fixed parameter A and a temperature-dependent wavelength, $\lambda_x(T)$. Some forms of the interpolation equation provided by this method are analytically invertible to calculate the estimated temperature. The effective wavelength method is thus widely used and is detailed in the next paragraph.

2.3. *Effective wavelength method*

The effective wavelength method uses a varying wavelength, called the extended effective wavelength, and is denoted by λ_x, which is calculated as a function of temperature. The interpolation equation based on Wien's law is given by the following equation:

$$\hat{I}_{\mathrm{D}} = A\ \exp\left(\frac{-C_2}{\lambda_x(T) \times T}\right), \tag{5}$$

where

$$\frac{1}{\lambda_x} = \frac{T}{C_2}\ \ln\left(\frac{\int_{\Delta\lambda} C_1\, W(\lambda)\lambda^{-5}\,\mathrm{d}\lambda}{\int_{\Delta\lambda} W(\lambda) L_0(\lambda, T)\,\mathrm{d}\lambda}\right).$$

Without the knowledge of W, an analytical extended effective wavelength versus the temperature should be suggested. Reference [10] suggests an extended effective wavelength which is expressed as a first order polynomial function of the inverse temperature. The Sakuma–Hattori interpolation equation is then given by

$$\hat{I}_{\mathrm{D}} = A\ \exp\left(\frac{-C_2}{b_0 \times T + b_1}\right), \tag{6}$$

where b_0 and b_1 are fitting parameters.

Reference [11] generalizes this formulation and the inverse of the extended effective wavelength is a polynomial function of the inverse temperature with different orders, as follows:

$$\frac{1}{\hat{\lambda}_x} = \sum_{i=0}^{N}\left(\frac{a_i}{T^i}\right) \tag{7}$$

where a_i are fitting parameters and N is the order of the polynomial function, which depends on the operating wavelength of the thermal imager, the spectral bandwidth of the filter, the temperature range and the required accuracy of the application. The interpolation equation formed using equations (5) and (7) is difficult to invert for high orders. However, when used with Wien's approximation, it can be fitted, to all orders, using linear least-squares techniques, unlike the Sakuma–Hattori equation which requires non-linear least-squares techniques. As shown in [16], for relatively narrow bandwidth thermal imagers, it is sufficient to use a polynomial function at first order ($N = 1$ and $a_2 = 0$) and the parameters a_0 and a_1 have a physical meaning and can be well approximated by equations (8) and (9) as follows:

$$a_0 = \frac{1}{\lambda_0}\left(1 + 6\left(\frac{\sigma_f}{\lambda_0}\right)^2\right) \tag{8}$$

$$a_1 = -\frac{C_2}{2\,\lambda_0^2}\left(\frac{\sigma_f}{\lambda_0}\right)^2, \tag{9}$$

where λ_0 and σ_f are the mean wavelength and standard deviation of the spectral responsivity of the thermal imager. If the ratio $r = \frac{\sigma_f}{\lambda_0} \ll 1$, the parameter a_0 will be close to the inverse of the mean wavelength of the spectral responsivity. The term a_1 describes the temperature dependence of the extended effective wavelength. The parameters a_0 and a_1 depend only on the mean wavelength and standard deviation of the spectral responsivity and they are independent of its shape (Gaussian, uniform, etc). Reference [12] provides a comprehensive study of the influence of r on the interpolation error. For wide bandwidth thermal imagers, the order N of equation (7) can be higher and at minimum the term a_2 is required.

3. Simulation of the interpolation error

A simulation study of the interpolation error is carried out with an interpolation equation (5) based on an extended effective wavelength equation (7) expressed as first and second order. The interpolation error is calculated, in the case of thermal imagers operating in NIR, for narrow and large bandwidths and for a wide temperature range from 300 °C to 1000 °C. The first aim is to highlight the variation of interpolation error in relation to the extended effective wavelength's order and the wide variation of the relevant parameter $r = \frac{\sigma_f}{\lambda_0}$, as in [12]. The second goal is to understand the influence of the noise due to experimental errors (non-linearity, non-uniformity, temporal noise, etc) on the interpolation error. This simulation analysis is carried out with noiseless and noisy data.

3.1. Simulation procedure

The simulated output signal I_D of the thermal imager is obtained according to equation (1) and therefore by integrating the product of the spectral responsivity of our thermal imager (W) with Planck's law. The parameter W is equal to the product of the spectral responsivity of the detector (set between 0 and 1), provided by the manufacturer, with the spectral distribution of the filters. The filters are Gaussian with a mean wavelength of $\lambda_0 = 1310\,\text{nm}$ and different full-width at half-maximum (FWHM), from 10 nm to 600 nm (which corresponds to a standard deviation $\sigma_f = \frac{\text{FWHM}}{\sqrt{8\ln 2}}$ varying from 4.24 nm to 254.8 nm). The relevant selected parameter, the ratio $r = \frac{\sigma_f}{\lambda_0}$, varies from 3.24×10^{-3} to 0.194. Finally, equation (1) is calculated over the temperature range from 300 °C to 1000 °C (respectively for a bandwidth $\Delta\lambda$ from 900 nm to 1700 nm).

For the second simulation, noise is optionally added to the output signal by defining $\check{I}_{D_j} = I_{D_j} + \nu_j$, where ν is the jth trial value of M trials ($j = 1 \ldots M$) for a random variable following a Gaussian distribution $\mathcal{N}(0, \sigma^2_{I_D})$ of mean zero and standard deviation σ_{I_D}.

The parameters of interpolation equation (5) are fitted to the previous simulated output signal, I_D or $\check{I}_D$, and to the reference temperature values T of Planck's law. The fit method is based on weighted least-squares fit where the weights are inversely proportional to the output signal values.

Finally, the estimated temperature $\hat{T}$ is calculated by the inverse of equation (5) and then by solving the polynomial equation (10) with Cardan's formula at third order.

$$\left(\frac{a_2}{\hat{T}^3}\right) + \frac{a_1}{\hat{T}^2} + \frac{a_0}{\hat{T}} - \frac{1}{C_2}(\ln(\hat{I}_D) - \ln(A)) = 0. \qquad (10)$$

The absolute interpolation error $E_T = |T - \hat{T}|$ and the maximum absolute interpolation error over all temperatures, $E_{T_{\text{peak}}}$, are then calculated. For noisy simulations, the mean value ($\bar{E}_T$) and the standard deviation (σ_{E_T}) of interpolation errors are calculated over M trials. The mean value over all temperatures is denoted $\bar{\bar{E}}_T$.

3.2. Influence of extended effective wavelength order

This first series of simulations is intended to study the influence of the extended effective wavelength's order in relation to the relevant parameter $r = \frac{\sigma_f}{\lambda_0}$. The simulation is carried out without noise on the output signal I_D. This approach clearly defines the dependence of the interpolation error on the order of the extended effective wavelength.

Figure 1 shows that the maximum absolute interpolation error, $E_{T_{\text{peak}}}$, decreases when the order of extended effective wavelength increases and when the ratio r decreases. At order zero, an interpolation error lower than 0.1 °C is achieved with a value of r lower than 9×10^{-3}, which corresponds to a FWHM of about 35 nm. At first order, the same value of the interpolation error is achieved for a value of r lower than 7×10^{-2}, or a FWHM value around 220 nm. Finally, at second order, the interpolation error is lower than 0.1°C for all the spectral bandwidths of the thermal imager.

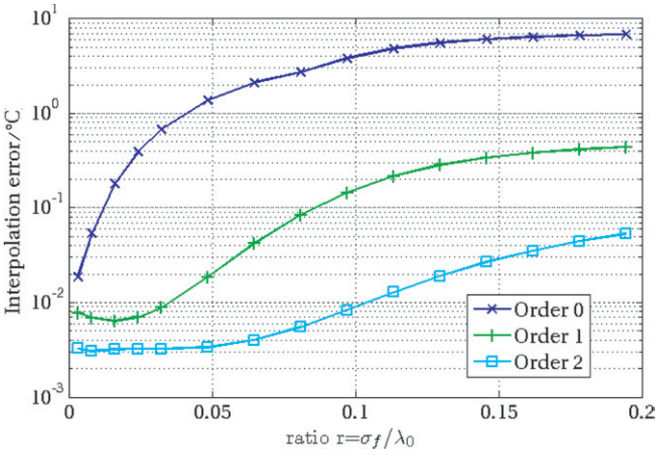

Figure 1. Logarithmic representation of the maximum absolute interpolation error, $E_{T_{\text{peak}}}$, versus the ratio $r = \frac{\sigma_f}{\lambda_0}$ for Gaussian filters with a mean wavelength of $\lambda_0 = 1310\,\text{nm}$ and standard deviation values from $\sigma_f = 4.2 \times 10^{-2}$ to 0.25.

As shown in table 1, and according to equation (4), the fitting parameter A increases with the bandwidth of the spectral responsivity of the camera. The increase, in absolute value, of the parameters a_0 and a_1 is also consistent with equations (8) and (9). The difference between the fitting values and the theoretical values remains low (a few per cent) as long as the value of r is lower than 0.05. The value of parameter a_2 is small with a narrow bandwidth filter and increases quickly with a wide bandwidth filter.

As a first conclusion and with noiseless data, a high order always decreases the interpolation error, and this decrease is even more significant for large values of r. For wide bandwidth filters, an interpolation equation with an extended effective wavelength at second order is the best choice to achieve an interpolation error of less than 0.1 °C.

3.3. Influence of noise

The second series of simulations are performed to study the influence of noise on the choice of the extended effective wavelength order.

The noisy output signal, $\check{I}_D$, is generated with a variation of relative standard deviation σ_{I_D} from 0% to 2% (for an output signal digitalized on 12 bits, the maximum relative standard deviation represents 80 DL). The number of trials is set to $M = 100$. This simulation is only performed with a wide bandwidth filter and with a value of r of 0.194 (for a mean wavelength of $\lambda_0 = 1310\,\text{nm}$ and a Gaussian filter, it corresponds to a FWHM value around 600 nm). This case induces a maximum difference of the interpolation error between an extended effective wavelength at first and second order.

For each M value of $\check{I}_D$, the temperatures are estimated with an interpolation equation with an extended effective wavelength at first and second order. Figure 2 shows the mean value of the interpolation error over the trials and temperatures, called $\bar{\bar{E}}_T$, for both orders. $\bar{\bar{E}}_T$ is very different when the relative standard deviation σ_{I_D} is lower than 1.5%. After

Table 1. Maximum temperature interpolation errors, $E_{T_{peak}}$, for each extended effective wavelength's order; fitting calibration parameter values for an extended effective wavelength at second order.

$1/\widehat{\lambda_x}$	0th order	1st order	2nd order				
r	$E_{T_{peak}}$/ °C	$E_{T_{peak}}$/ °C	A/ (DL s^{-1})	a_0/ µm^{-1}	a_1/ (K µm^{-1})	a_2/ (K^2 µm^{-1})	$E_{T_{peak}}$/ °C
3.24×10^{-3}	0.0187	0.006442	25.40×10^4	0.7638	−0.4051	93.843	30.76×10^{-4}
1.13×10^{-2}	0.0941	0.006533	89.038×10^4	0.76426	−0.8555	95.954	30.91×10^{-4}
7.46×10^{-2}	2.499	0.06529	61.22×10^5	0.7888	−24.927	19.79×10^2	47.91×10^{-4}
0.194	6.804	0.441	14.151×10^6	0.825	−82.38	13.69×10^3	53.46×10^{-2}

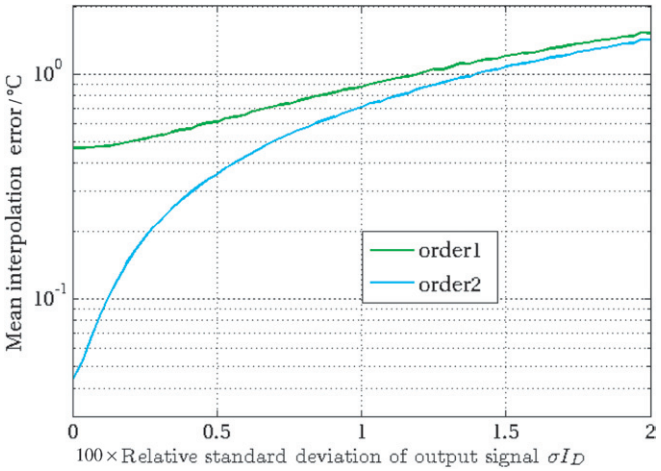

Figure 2. Logarithmic representation of $\bar{\bar{E}}_T$ versus the relative standard deviation of the noise of the output signal σ_{I_D} for a Gaussian filter with a ratio $r = 0.194$ (mean wavelength of $\lambda_0 = 1310$ nm and FWHM of 600 nm).

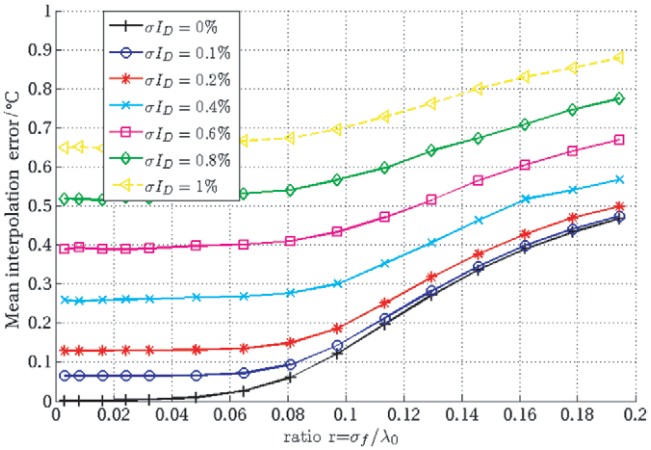

Figure 3. Mean (over the trials and temperatures) of interpolation errors for an extended effective wavelength at first order versus the ratio r of a Gaussian filter (mean wavelength of $\lambda_0 = 1310$ nm and FWHM from 10 nm to 600 nm) and for seven levels (from 0% to 1%) of the relative standard deviation of the noise of the output signal.

this value, the quantity $\bar{\bar{E}}_T$ becomes similar for both cases. A second-order extended effective wavelength significantly reduces the interpolation error only if the noise standard deviation of the output signal is lower than 1.5%. With a very noisy output signal, when the relative standard deviation σ_{I_D} is above 1.5%, an increase in the order of the extended effective wavelength moderately improves the interpolation error.

As a second conclusion, for low-noise data, the largest part of the interpolation error is due to the interpolation equation. An extended effective wavelength at second order significantly reduces the interpolation error. In contrast, for high-noise data, a second order does not seem to provide improvements. The next paragraph studies the contribution of the second-order extended effective wavelength for high-noise signals.

3.4. Coupled influence of order and noise

The third series of simulations extends the previous results to the entire range of variation of parameter r (from 3.24×10^{-3} to 0.194) and with a variation of relative standard deviation σ_{I_D} of the output signal from 0% to 1%. The number of trials is set at $M = 100$.

Figures 3 and 4 confirm that the quantity $\bar{\bar{E}}_T$ increases with the ratio r and with the noise of the output signal. The mean interpolation error obtained with an extended effective wavelength at first or second order is always greater than 0.1 °C for a relative standard deviation higher than 0.15%, whatever

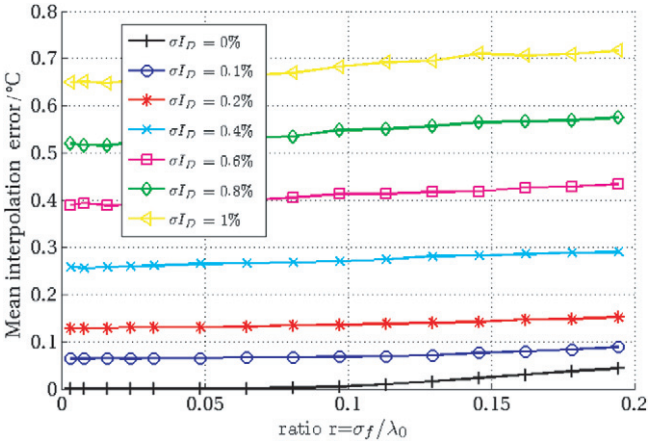

Figure 4. As for figure 3 but with an interpolation equation with an extended effective wavelength at second order.

the value of r. Above this value, the interpolation error is mainly due to the noise in the output signal.

However, the quantity $\bar{\bar{E}}_T$ increases faster with the ratio r for an extended effective wavelength at first order than it does at second order. It reaches 0.79 °C at order 1 for a relative standard deviation $\sigma_{I_D} = 1\%$ and for a ratio $r = 0.194$. For the same configuration, the quantity $\bar{\bar{E}}_T$ for an extended effective wavelength at second order rises to 0.59 °C. Figure 5 demonstrates that the difference between quantity $\bar{\bar{E}}_T$ for an

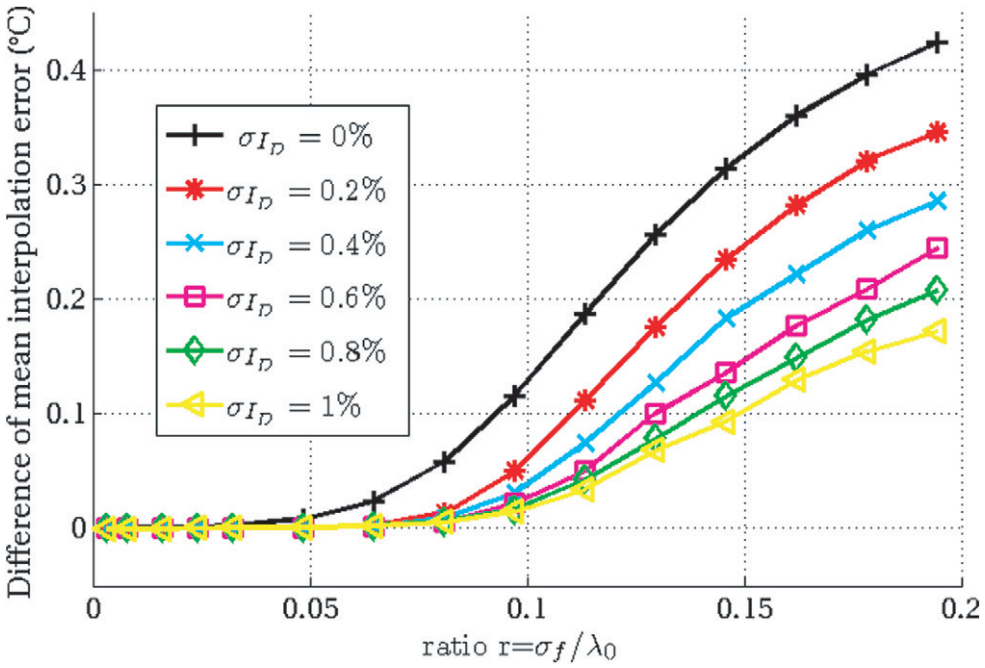

Figure 5. Difference of interpolation errors averaged over the trials and temperatures for an extended effective wavelength at first and second order versus the ratio r of a Gaussian filter (mean wavelength of $\lambda_0 = 1310$ nm and FWHM from 10 nm to 600 nm) and for six levels (from 0% to 1%) of the relative standard deviation of the noise of the output signal.

interpolation equation with an extended effective wavelength at first and second order, denoted $\Delta\bar{\bar{E}}_T = \bar{\bar{E}}_T(\text{order } 1) - \bar{\bar{E}}_T(\text{order } 2)$, is always positive.

As a third conclusion, an interpolation equation with an extended effective wavelength at second order is always more efficient than it is with one at first order. As this positive difference increases with the ratio r, an extended effective wavelength at second order is always advisable with wide bandwidth filters. However, this benefit decreases when the noise standard deviation on the output signal increases. For example, for the highest values of parameter $r = 0.194$, the second order brings an additional accuracy of about 0.43 °C compared with the first order. When the noise reaches 1%, this performance decreases to only 0.2 °C. For very noisy signal, and for applications involving high time resolution, a second-order parametrization of the extended effective wavelength may not be the best compromise.

4. Experimental validation of the interpolation error

To compare simulation with experimental results, the interpolation equation with an extended effective wavelength at first or second order is fitted from measured data provided by a near infrared thermal imager.

The calibration methodology, involving a black body and the thermal imager, is described in the first paragraph. Compared with the simulation step, the thermal imager can be seen as a matrix of detectors and each detector as a thermometer. Then, the interpolation equation is fitted from the output signal of each detector. However, this signal is not ideal and some departures from ideal behaviour are characterized in the second paragraph. Finally, the interpolation error of each detector is determined in two configurations of calibration: the thermal imager equipped with a narrow Gaussian filter and without it (i.e. on the entire spectral band of the thermal imager). The mean value of this interpolation error field is compared with simulation results.

4.1. Experimental set-up

The calibration set-up is composed of a thermal imager aligned with a black body on a translation stage.

The easiest way to calibrate the thermal imager is to illuminate it uniformly so that each pixel receives the same flux. A flat-plate calibrator or a system based on an integrating sphere would offer such an illumination compatible with the field of view of the imager. Unfortunately, the flat-plate calibrator cannot provide a reference temperature up to 500 °C, which is necessary to calibrate the near infrared thermal imager, and an integrating sphere would complicate the experimental set-up. The calibration of the thermal imager is then carried out with a cavity black body with relatively small aperture size in relation to the field of view of the thermal imager. It provides reference temperatures over the range 50 °C to 1200 °C with a cavity diameter of 50 mm and an emissivity of 0.995. The NIR lens used has a 50 mm focal length and the distance between the thermal imager and the black body is around 1 m. The advantage of this calibration is the reliable, high and constant emissivity of the cavity black body. The major drawback is that the aperture only fills a relatively small part of the image (25% or 20 000 pixels). In order to assess the entire image it is necessary to carry out multiple measurements with the source positioned at different points within the image. In this paper, only one position is shown. The temperature of the black body is measured by

a reference S-type thermocouple. The experimental set-up is located in a black room to minimize surrounding radiation.

The thermal imager is a 320×256 InGaAs array operating in the near infrared spectral band from 0.9 µm up to 1.7 µm and with a Peltier cooler. The set-up includes a filter wheel with three Gaussian filters, a black screen and an empty hole. The wheel is motorized to rotate and is piloted by the software. For this experiment, the mean wavelength is $\lambda_0 = 1310$ nm with a FWHM of 50 nm for the narrow filter considered and a FWHM of 600 nm without filters. The thermal imager is equipped with a lens of focal length 50 mm and the F-number is set to 4. The exposure time range available is between 1 µs and 400 s. However, the minimum time is limited to 100 µs to minimize the non-linearity of the signal with the exposure time, and the maximum time is limited to 1 s to minimize the duration of the calibration. Consequently, the calibration temperature range is limited between 500 °C and 850 °C, which is lower than the range used for the simulations. As shown in reference [12], for the Sakuma–Hattori equation and when the temperatures are equally spaced, the peak interpolation error increases as the cube of the temperature range. The values of the simulated and measured interpolation errors will not be the same. However, trends are comparable, which validates the noise impact on the interpolation equation.

4.2. Evaluation of thermal imager signal

The thermal imager is an array device composed of many detectors. Its behaviour is a composition of the individual behaviour of each detector, and of their juxtaposition.

As a single detector, the output signal of each detector is given by the sum of three terms: signal due to the radiation source, noise signal from the dark current and offsets and the signal produced by temporal noises. The ambient radiation entering the black body can be neglected above 500 °C.

The dark current and the offsets are part of the signal acquired in darkness. This signal, denoted $I_{\mathrm{D}}^{\mathrm{dark}}$, can be subtracted from the signal obtained during the illumination with the radiation source, denoted I_{D}.

Moreover, the exposure time ti is managed to avoid the thermal imager signal becoming lower than the noise level and to avoid overexposure. When a detector is illuminated with sufficient radiance, the exposure time is then calculated to obtain a signal level around 75% of the maximum value. Around this value and for the limited exposure time chosen, the signal of each detector is linearly dependent on the exposure time.

Under these conditions, the corrected signal for each detector of coordinates u and v, denoted $I_{\mathrm{D}}^{\mathrm{c}}(u, v)$, is calculated from the difference between the signal under illumination, I_{D}, and the dark signal, $I_{\mathrm{D}}^{\mathrm{dark}}$, and is normalized by the exposure time, as given in equation (11).

$$I_{\mathrm{D}}^{\mathrm{c}}(u, v) = \frac{I_{\mathrm{D}}(u, v) - I_{\mathrm{D}}^{\mathrm{dark}}(u, v)}{ti} \tag{11}$$

The effects of temporal noise are minimized by averaging the corrected signal over several frames (in practice 50 frames). The histogram plotted in figure 6 shows the dispersion of the

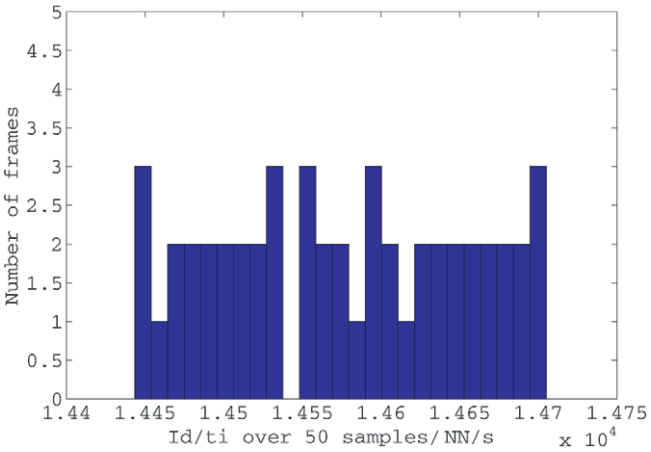

Figure 6. Histogram over fifty samples of corrected signal of equation (11) for a black-body temperature at 500 °C.

corrected signal for a central pixel. The temporal mean $\bar{I}_{\mathrm{D}}^{\mathrm{c}}$ and its associated standard deviation, denoted $\sigma_{I_{\mathrm{D}}^{\mathrm{c}}}$, are calculated. The values are recorded for a black-body temperature of $T = 500$ °C and without filter. Considering the noise as independent of the temperature, this measurement gives the minimum signal-to-noise ratio and represents the worst situation. The standard deviation of the corrected signal is low (around $\sigma_{I_{\mathrm{D}}^{\mathrm{c}}} = 0.5\%$), and therefore the mean value represents an accurate representation of each detector's value. It should be noted that this standard deviation, with a $\lambda_0 = 1.3$ µm monochromatic thermal imager, corresponds to a temperature uncertainty of $\Delta_T = \frac{T^2 \lambda_0}{C_2} \sigma_{I_{\mathrm{D}}^{\mathrm{c}}} = 0.27$ °C at a temperature of $T = 500$ °C. As our thermal imager is not monochromatic, the measured error would be higher than this value.

As a device array, additional factors need to be investigated, such as image non-uniformity and size-of-source effect (SSE). Firstly, the calculation of the corrected signal compensates the non-uniformity due to dark current and offsets. Secondly, the residual non-uniformity is due to the difference in responsivity of each detector, denoted $W(u, v)$ in equation (1). This can be taken into account by a calibration of each detector across the calibration parameter A. To do so, the responsivity of each detector has to be assumed to be independent and therefore the SSE and the cross-talk problem must be negligible. It should be noted that this calibration is performed under the same conditions as our application [5], for which the temperature measurement is carried out on a target with the same size as the black-body aperture and at the same distances. These two phenomena are therefore assessed over a range of distances in the depth of field of the thermal imager and with the image well focused. The central area is then well overfilled by the aperture of the black body at a fixed temperature of 700 °C. Under these conditions of a small change in angular black-body aperture, the signal indicated by the detectors within the central area of the black body slightly increases as the black-body distance decreases. The variation in the level of mean value of the corrected value is less than 0.5%. As a consequence, correction of SSE is not applied, and the imperfections of optical components and the cross-talk problem can be neglected. The response of each detector is then assumed to be independent.

Table 2. Mean spatial and standard deviations values of fitting parameters with an extended effective wavelength at first and second order for a narrow bandwidth filter with a FWHM of 50 nm and a mean wavelength of $\lambda_0 = 1310$ nm.

$\frac{1}{\tilde{\lambda}_x}$	$\tilde{A}/(\mathrm{DL\,s^{-1}})$	$100 \times \sigma_A$	$\tilde{a_0}/\mu\mathrm{m}^{-1}$	$100 \times \sigma_{a_0}$	$\tilde{a_1}/(\mathrm{K\,\mu m^{-1}})$	$100 \times \sigma_{a_1}$	$\tilde{a_2}/(\mathrm{K^2\,\mu m^{-1}})$	$100 \times \sigma_{a_2}$
1st order	2.264×10^{11}	1.91	0.765	0.38	−4.48	5.41	—	—
2nd order	1.84×10^{11}	2.14	0.761	1.85	−34.42	3.2	1.95×10^4	3.2

As a conclusion, the radiometric calibration of the thermal imager is equivalent to the calibration of each detector. Each detector produces a corrected signal that can be calibrated independently of the others, and all can be calibrated together at the same time. The calibration signal of each detector is the temporally averaged signal, denoted $\bar{I}_{\mathrm{D}}^{\mathrm{c}}$:

$$\bar{I}_{\mathrm{D}}^{\mathrm{c}}(u, v) = \frac{A}{\exp\left(\frac{C_2}{\lambda_x(T,u,v)\times T}\right)} \tag{12}$$

with

$$\frac{1}{\lambda_x(T, u, v)} = a_0(u, v) + \frac{a_1(u, v)}{T}\left(+\frac{a_2(u, v)}{T^2}\right). \tag{13}$$

The calibration depends on three or four images of fitting parameters, $A(u, v)$, $a_0(u, v)$, $a_1(u, v)$ and $a_2(u, v)$, that are determined during the radiometric calibration process.

4.3. Interpolation error of the thermal imager with a Gaussian filter with a FWHM of 50 nm

For a thermal imager equipped with a Gaussian filter with a FWHM of 50 nm and a mean wavelength of $\lambda_0 = 1310$ nm, the first calibration procedure is carried out measuring the corrected signal from equation (11) and knowing the black body temperatures ranging from 500 °C to 850 °C with an increment of 25 °C. Hence, three or four images of the calibration parameters ($A(u, v)$, $a_0(u, v)$, $a_1(u, v)$ and $a_2(u, v)$) of interpolation equation (12) with an extended effective wavelength at first and second order are fitted. The parameter values are then computed for each detector of coordinates (u, v) in the area illuminated by the black body. It should be noted that the detectors outside the area of the black body are not calibrated.

The mean spatial value, denoted $\tilde{A}$, $\tilde{a_0}$, $\tilde{a_1}$ and $\tilde{a_2}$ and the standard deviations, denoted σ_A, σ_{a_0}, σ_{a_1} and σ_{a_2} of calibration parameters are tabulated in table 2.

The relative standard deviation of the parameter A is around 2%. This value shows the low non-uniformity of the detector's responsivity (see equation (4)). For the calibration parameters $\tilde{a_0}$ and $\tilde{a_1}$, the experimental values are close to the theoretical values (see table 1). According to equation (8), the inverse of the parameter $\tilde{a_0}$ is homogeneous to the mean wavelength of the filter, λ_0 (when $\frac{\sigma}{\lambda_0} \ll 1$), which is equal to 1307 nm. This value can be compared with the value of the mean wavelength of the filter, which is equal to 1310 nm. Even in calibration experiments with a noisy signal of the thermal imager, this comparison demonstrates the physical consistency of the behaviour of the interpolation equation with two orders of the extended effective wavelength. The low values of standard deviations, 0.38% for σ_{a_0} and 5.41% for σ_{a_1}, again show the small spatial dispersion of the detector's sensitivity.

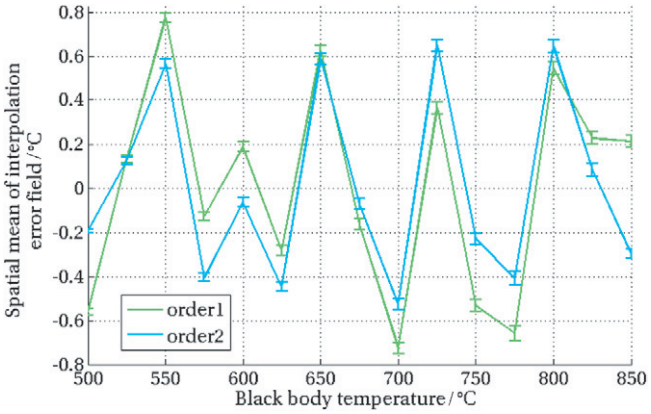

Figure 7. Values of mean ($\tilde{E_T}$) and standard deviation (σ_{E_T}) of the interpolation error field versus the temperature for a Gaussian filter with a FWHM of 50 nm and a mean wavelength of $\lambda_0 = 1310$ nm.

Next, for each detector, the field of estimated temperatures $\hat{T}(u, v)$ is calculated by the resolution of the polynomial equation (10). The field of interpolation errors $E_T(u, v) = T - \hat{T}(u, v)$ is calculated. Its mean spatial value, denoted $\tilde{E_T}$, and its standard deviation, denoted σ_{E_T}, across the calibrated detectors, are calculated. Figure 7 shows the mean spatial value versus the black-body temperature T. Error bars represent the standard deviation of interpolation error with an extended effective wavelength at first and second order.

The mean spatial value of interpolation errors, $\tilde{E_T}$, calculated with an interpolation equation with an extended effective wavelength at first order is similar to the one calculated for an extended effective wavelength at second order. For an interpolation equation with an extended effective wavelength at first order (respectively at second order), the standard deviation σ_{E_T} is between 2.7% and 12% (respectively between 2.3% and 10%).

Finally, the absolute mean value over all temperatures, denoted $\bar{\tilde{E}}_T$, of the spatial mean value $\tilde{E_T}$ is slightly lower for an extended effective wavelength at second order ($\bar{\tilde{E}}_T = 0.33\,^{\circ}\mathrm{C}$) than for an extended effective wavelength at first order ($\bar{\tilde{E}}_T = 0.407\,^{\circ}\mathrm{C}$). These values are consistent with those calculated in the previous section with simulated noisy output signal, $\check{I}_{\mathrm{D}}$, with a standard deviation of noise of $\sigma_{I_{\mathrm{D}}} = 0.5\%$. This value is also consistent with the temporal standard deviation of the corrected signal (see figure 6).

For a thermal imager with a standard deviation of noise around of $\sigma_{I_{\mathrm{D}}} = 0.5\%$ equipped with a narrow bandwidth Gaussian filter, and even for a large temperature range, an

Table 3. As for table 2 but for a thermal imager without filter.

$\frac{1}{\lambda_x}$	$\tilde{A}/(\mathrm{DL\,s^{-1}})$	$100 \times \sigma_A$	$\tilde{a_0}/\mu\mathrm{m}^{-1}$	$100 \times \sigma_{a_0}$	$\tilde{a_1}/(\mathrm{K\,\mu m^{-1}})$	$100 \times \sigma_{a_1}$	$\tilde{a_2}/(\mathrm{K^2\,\mu m^{-1}})$	$100 \times \sigma_{a_2}$
1st order	3.78×10^{13}	0.85	1.16	0.091	−217.39	0.207	—	—
2nd order	8.84×10^{13}	5.26	1.39	0.47	−446.62	0.81	8.211×10^4	0.97

interpolation equation with an extended effective wavelength at first order can be a good approximation to achieve a low interpolation error. A higher order of the extended effective wavelength moderately improves the interpolation error. These experimental results confirm the simulated results of figure 5 in which, for $r \ll 1$, the difference in interpolation errors with an extended effective wavelength at first and second order is very low.

4.4. Interpolation error of the thermal imager over its entire bandwidth

The second calibration was carried out for a thermal imager over its entire bandwidth (0.9 µm to 1.7 µm), without any filter, and with the same calibration procedure as previously used.

The spatial mean and standard deviation values of the image's calibration parameters ($A(u, v)$, $a_0(u, v)$, $a_1(u, v)$ and $a_2(u, v)$) of the interpolation equation with an extended effective wavelength at first and second order are tabulated in table 3.

Compared with the case of the narrow Gaussian filter, the value of $\tilde{A}$ is high. According to equation (4), the value of the integral over the spectral bandwidth increases with the bandwidth, as it does for $\tilde{a_0}$ and $\tilde{a_1}$, due to the fact that the standard deviation of the spectral responsivity of the thermal imager is wider. The thermal imager has a rectangular spectral responsivity from 0.9 µm to 1.7 µm. In this case of a wide bandwidth, the value of the calibration parameter $\tilde{a_2}$ is also very high. This value justifies the choice of an interpolation equation at a higher order. It should be noted that for this calibration, the standard deviation values are also very low.

The mean spatial values, denoted $\tilde{E_T}$, of the interpolation error field are shown versus the black body temperature T in figure 8 for an interpolation equation with an extended effective wavelength at first and second orders. The error bars represent the standard deviation, denoted σ_{E_T}.

An interpolation equation with an extended effective wavelength parametrized at first order involves a higher interpolation error than for the first order. It reaches an interpolation error up to one degree for a few temperatures. In contrast, an interpolation equation with an extended effective wavelength at second order limits the interpolation error around a mean value over all temperatures of $\bar{\tilde{E}}_T = 0.36\,^\circ\mathrm{C}$. The second order shows a significant improvement in the value of the temperature error ($\bar{\tilde{E}}_T = 0.73\,^\circ\mathrm{C}$ for first order versus $\bar{\tilde{E}}_T = 0.36\,^\circ\mathrm{C}$ for second order). In this case, the interpolation error depends on the order of the extended effective wavelength. This result has already been noted in figure 5 when the value of r increases.

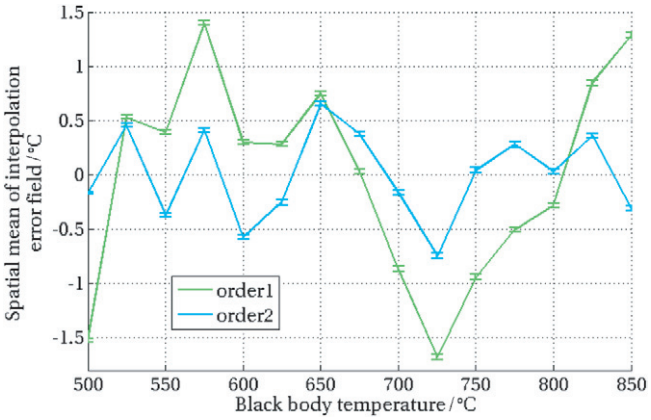

Figure 8. As for figure 7 but for a thermal imager without filter.

4.5. Comparison of the simulated and measured interpolation errors

The two previous experiments confirm the trends observed in figure 5, and in this paragraph, our approach is to compare the values of simulated and measured interpolation errors. The simulation is performed with simulated noisy output signal, $\check{I}_\mathrm{D}$, which is generated with the measured relative standard deviation σ_{I_D} on the signal from the thermal imager which is around 0.5% (see figure 6). The standard deviation of the imager's spectral responsivity σ_f varies and the variation of the ratio $r = \frac{\sigma_f}{\lambda_0}$ is from 3.24×10^{-3} to 0.194. This simulation is intended to represent the interpolation error in a configuration similar to that of the thermal imager. Figure 9 shows the quantity $\bar{\tilde{E}}_T$ for simulated interpolation errors with an interpolation equation with an extended effective wavelength at first and second order. In this figure, the measured interpolation errors, $\bar{\tilde{E}}_T$, are also reported.

For an extended effective wavelength at second order, the measured interpolation errors are consistent with the simulated ones for a standard deviation of noise in the output around $\sigma_{I_\mathrm{D}} = 0.5\%$. For an extended effective wavelength at first order, the measured interpolation errors are higher than the simulated ones with the same standard deviation of noise in the output signal. The measured values should correspond to a higher standard deviation of noise in the output around $\sigma_{I_\mathrm{D}} = 0.6\%$. This result demonstrates that for middle-noise on the output signal, an extended effective wavelength at second order provides lower residual fits on the fitting parameters A, a_0 and a_1.

As a conclusion, for our thermal imager with a middle-noise on the output signal, for a ratio $r < 0.07$, an extended effective wavelength at second order slightly improves the interpolation error (around 0.07 °C) with measured data, unlike the conclusions reached with simulated data in the previous

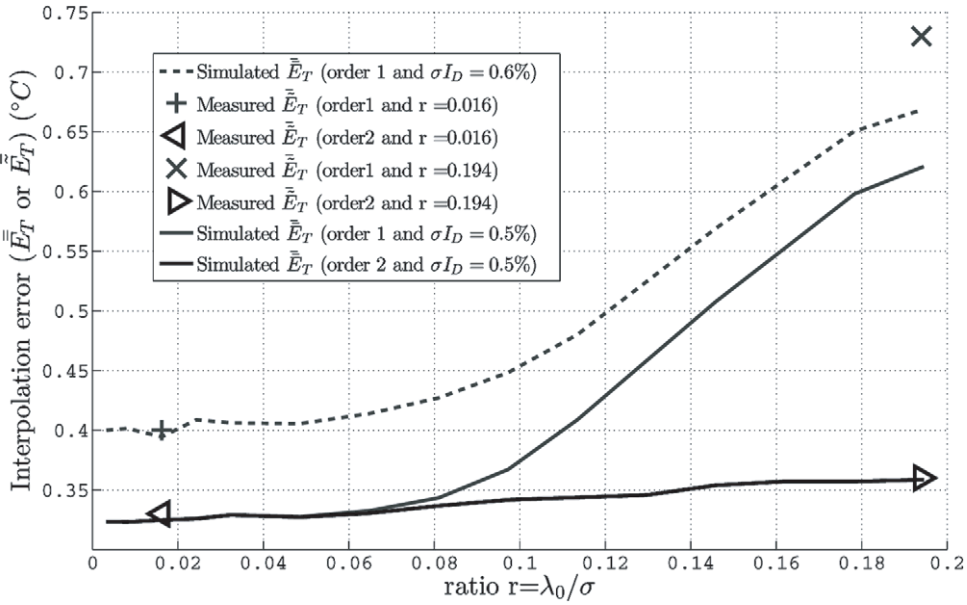

Figure 9. Quantities $\bar{\bar{E}}_T$ or $\bar{\bar{E}}_T$ versus the ratio r for the noise's relative standard deviation of the output signal $\sigma_{I_D} = 0.5\%$ and $\sigma_{I_D} = 0.6\%$.

section. For a ratio up to $r > 0.07$, as demonstrated with simulated data, only an interpolation equation with an extended effective wavelength at second order involves a significant improvement in the value of the interpolation error.

5. Conclusion

This paper has described the application of an interpolation equation with a temperature-dependent effective wavelength for the calibration of near infrared thermal imagers (see equation (5)). This dependence is defined as follows: the inverse extended effective wavelength is a polynomial function of the inverse temperature (see equation (7)). The order of the function mainly depends on the mean wavelength and the standard deviation of the imager's bandwidth, the temperature range and the accuracy required.

For temperatures ranging from 300 °C to 1000 °C, a simulation performed with a free noise signal of the thermal imager showed that the interpolation error was lower than 0.1 °C if the filter's FWHM was lower than 220 nm (for a temperature-dependent effective wavelength at first order and a mean wavelength of 1310 nm). Using an effective wavelength at second order, the FWHM could be extended to 600 nm.

A second simulation with a noisy signal of the thermal imager gave the interpolation error in relation to the percentage of noise and the characteristics of the imager's bandwidth. This simulation showed that an interpolation equation with an effective wavelength at second order decreases the interpolation error with noise. However, the interpolation error was not negligible and was lower than 0.1 °C only for a filter bandwidth lower than 30 nm.

The simulations were compared with experimental results obtained by a thermal imager with a noise standard deviation around 0.5% and equipped with a narrow bandwidth filter (FWHM of 50 nm). An interpolation equation with an effective wavelength, at first or second order, provided a comparable interpolation error which was around 0.3 °C. However, for wider spectral bandwidth filters (FWHM higher than 50 nm), an effective wavelength at second order was required to keep a low value of interpolation error.

The interpolation equation with an extended effective wavelength, at first and second orders, was implemented in an original method [5] for measuring the true temperature field by fusing the radiance temperature and the reflectivity measurement fields.

Acknowledgments

This work was carried out in the context of the R3T (Real Time True Temperature) project, supported by the French National Research Agency.

References

[1] Mayrhofer F, Zauner G, Hendorfer G, Darilion G and Müller T 2008 Optical characterization of thin layers grown on metal components *Proc. SPIE* **7003** 70030R
[2] Rotrou Y 2006 Thermographie courtes longueurs d'onde avec des caméras silicium: contribution à la modélisation radiométrique *PhD Thesis* Ecole nationale supérieure de l'aéronautique et de l'espace, CROMeP, Albi
[3] Mansouri A, Marzani F, Hardeberg J and Gouton P 2005 Optical calibration of a multispectral imaging system based on interference filters *Opt. Eng.* **44** 027004
[4] Meriaudeau F 2007 Real time multispectral high temperature measurement: application to control in the industry *Image Vis. Comput.* **25** 1124–33
[5] Sentenac T, Gilblas R, Hernandez D and Le Maoult Y 2012 Bi-color near infrared thermoreflectometry: a method for true temperature field measurement *Rev. Sci. Instrum.* **83** 124902
[6] Ferrero A, Campos J and Pons A 2006 Low-uncertainty absolute radiometric calibration of a CCD *Metrologia* **43** 17
[7] Kostkowski H J and Lee R D 1962 *Theory and Methods of Optical Pyrometry* (Princeton, NJ: Van Nostrand-Reinhold)

[8] Bezemer J 1974 Spectral sensitivity corrections for optical standard pyrometers *Metrologia* **10** 47
[9] Hahn J W and Rhee C 1994 Interpolation equation for the calibration of infrared pyrometers *Metrologia* **31** 27
[10] Sakuma F and Hattori S 1982 Establishing a practical temperature standard by using a narrow-band radiation thermometer with a silicon detector *Temperature: its Measurement and Control in Science and Industry* vol 5 ed J F Schooley (New York: AIP) pp 421–7
[11] Saunders P 1997 General interpolation equations for the calibration of radiation thermometers *Metrologia* **34** 201–10
[12] Saunders P and White D R 2004 Interpolation errors for radiation thermometry *Metrologia* **41** 41
[13] Campos J, Corréons A, Pons A, Corredera P, Fontecha J L and Jiménez J 2001 Spectral responsivity uncertainty of silicon photodiodes due to calibration spectral bandwidth *Meas. Sci. Technol.* **12** 1926–31
[14] Rotrou Y, Sentenac T, Le Maoult Y, Magnan P and Farré J 2006 Near infrared thermography with silicon FPA—comparison to MWIR and LWIR thermography *Quant. Infrared Thermogr. J.* **3** 93–115
[15] Coates P B 1977 Wavelength specification in optical and photoelectric pyrometry *Metrologia* **13** 1–5
[16] Saunders P and White D R 2003 Physical basis of interpolation equations for radiation thermometry *Metrologia* **40** 195